STELLAR EVOLUTION. I. THE APPROACH TO THE MAIN SEQUENCE*

ICKO IBEN, JR.
California Institute of Technology, Pasadena, California
Received August 18, 1964; revised November 23, 1964

ABSTRACT

The manner in which nuclear reactions replace gravitational contraction as the major source of stellar luminosity is investigated for model stars of population I composition in the mass range $0.5 < M/M_\odot < 15$ 0. By following in detail the depletion of C^{12} from high initial values down to values corresponding to equilibrium with N^{14} in the C-N cycle, the approach to the main sequence in the Hertzsprung-Russell diagram and the time to reach the main sequence, for stars with $M \geq 1.25\ M_\odot$, are found to differ significantly from data reported previously.

I. INTRODUCTION

This is the first in a series of investigations which follow the evolution of popuation I stars from stages of gravitational contraction through hydrogen- and helium-burning stages. The objective of this paper is to describe in detail the manner in which pre-main-sequence gravitational contraction is replaced by nuclear burning as the primary source of stellar energy. Preliminary results have been previously reported by Iben (1963*b*).

By not assuming *ab initio* that C^{12} is in equilibrium with creating and depleting reactions, several interesting new features appear. In all models with $M \geq M_\odot$, a convective core grows and then recedes in mass as C^{12} first begins to burn and then is depleted from initial values down to equilibrium values in the deep interior. For stellar masses in excess of $1.25\ M_\odot$, double luminosity maxima and minima appear in the evolutionary path near the main sequence. The path from the first maximum to the first minimum is associated with the onset of C^{12} burning as the star attempts to settle onto a "$C^{12}(p, \gamma)$-burning" main sequence. The approach to the second maximum is the result of further gravitational contraction as C^{12} is rapidly reduced to equilibrium values near the center. The final minimum represents the standard main-sequence state in which the full p-p and C-N cycle reactions have replaced gravitational contraction as the source of escaping energy.

By avoiding the restrictive assumption of homologous changes (Hayashi 1961; Cameron 1962; Weymann and Moore 1963) the gravitational contraction time for a star of solar mass is found to be close to the classical Kelvin-Helmholtz contraction time. Due in part to the waiting time accompanying the depletion of C^{12}, stars more massive than $1.25\ M_\odot$ require longer to reach the standard main sequence than would have been the case of C^{12} had been assumed to be in equilibrium at all times, as was done in the work of Henyey, LeLevier, and Levée (1955).

II. INITIAL MODELS AND BASIC PROCEDURES

Initial models are constructed by means of classical fitting techniques: center-outward integrations are matched with surface-inward integrations. Central temperatures are chosen low enough that nuclear energy-generation rates are negligible relative to gravitational energy-generation rates, but high enough that hydrogen and helium are ionized throughout most of the star. It is assumed that the effective energy-generation rate varies

* Supported in part by the National Aeronautics and Space Administration and the Office of Naval Research.

as the first power of the temperature: that is, $\epsilon = CT$, where C is a parameter independent of the position in the star. For a given mass, two static models are constructed with slightly different values of C. The model with the larger value of C has the smaller binding energy, the larger radius, and, in general, the higher luminosity. It therefore precedes in time the model with the smaller value of C. The time separation between the two models is determined by dividing the difference in binding energy by the sum of the luminosities of the two models.

If the two models so constructed are fully convective, they are also exact solutions of the complete time-dependent equations describing the stellar interior. The reason for this is clear. The local rate of conversion of gravitational energy into escaping energy is $\epsilon_g = -T\,dS/dt$, where dS/dt is the time derivative of entropy per gram and ϵ_g is the compressional work done per gram per second reduced by the increase in thermal energy per gram per second (see Appendix B). In a fully convective region in which the temperature gradient is only slightly in excess of the local adiabatic temperature gradient, entropy per gram is independent of position. Thus, the derivative dS/dt is also independent of position and the effective rate of energy generation during stages in which the star is in adiabatic equilibrium throughout is exactly $\epsilon_g = C(t)T$, where $C(t)$ varies only with time.

For $M \leq 3\,M_\odot$, the initial models presented here are fully convective. Initial models of larger mass possess small radiative cores. For them, the assumption $\epsilon = CT$ is not justified. However, the error initially introduced damps out rapidly as evolutionary calculations proceed.

At the start of evolutionary calculations, the two initial models are each broken into an interior and an envelope. The mass in the envelope is chosen large enough that the envelope extends inward beyond the subsurface region where the superadiabatic gradient is large (see, e.g., Iben 1963*a*), but small enough that very little energy is either absorbed or generated within the envelope during evolution. The interior is broken up into mass shells in such a way that the fractional change in any variable across a shell is less than 10 per cent. Evolutionary calculations are then instituted following a modification of the implicit-difference method described by Henyey, Forbes, and Gould (1964). Details of modifications are described in Appendix A. The physics included in the static envelope solutions, which provide an outer boundary condition for the time-dependent interior solutions, are described by Iben (1963*a*).

Transmutations among the six "primary" nuclear species H^1, He^3, He^4, C^{12}, N^{14}, and O^{16} are followed in detail during evolution. The "secondary" elements H^2, Li^7, Be^7, B^8, N^{13}, C^{13}, O^{15}, N^{15}, F^{17}, and O^{17} are assumed to be destroyed as rapidly as they are formed. Although these secondary nuclear species are not followed explicitly, the change in the primary species as well as the energy released as a result of "fast" transformations are properly taken into account. Pertinent reaction rates and energy-generation rates may be found in Appendix B. The reaction $C^{13}(p, \gamma)N^{14}$ is not, properly speaking, fast relative to the $C^{12}(p, \gamma)N^{13}$ reaction. However, the circumstance that, over all densities and temperatures encountered, the lifetime of a C^{13} nucleus against proton capture is nearly constant (four times shorter) relative to the lifetime of a C^{12} nucleus against proton capture, permits C^{13} to be treated as a secondary element, particularly if initial composition is chosen so that $N(C^{13})/N(C^{12}) = 0.25$.

The initial distribution by mass among the six primary species is chosen to be $X_1 = 0.708$, $X_3 = 0.0$, $X_4 = 0.272$, $X_{12} = 0.00361$, $X_{14} = 0.00120$, and $X_{16} = 0.0108$. Opacity in the interior is taken from Iben and Ehrman (1962) with the choice of $Z = 0.02$ as the total mass fraction of heavy elements. Opacity in regions of partial hydrogen ionization is taken from Kippenhahn, Temesvary, and Bierman (1958) in the form used by Iben (1963*a*). The ratio of mixing length to density scale height in the envelope is fixed for all models at $\frac{1}{2}$.

III. EVOLUTION AT ONE SOLAR MASS

The solid curve in Figure 1 describes the evolutionary path a of 1 $M\odot$ star in the theoretical H-R diagram (log L vs. log T_e, luminosity L in units of 3.86×10^{33} erg/sec and surface temperature T_e in units of degrees Kelvin). A larger portion of the track is shown in Figure 17 (see below). Over the major portion of the almost vertical segment of the track, the star is dominantly convective (a radiative core begins to grow when log $L \lesssim 0.45$). Luminosity and surface temperature are therefore very sensitive to the opacity in the extremely narrow photospheric layers of the star. Contrary to the situation prevailing during most nuclear burning phases, evolution is considerably influenced by variations in surface conditions.

At the very low surface temperatures ($\sim$4000° K) encountered during the early contracting phases, the major contribution to the opacity in photospheric layers is absorption by the H^- ion, electrons to form this ion being supplied by metals of low ionization potential. To illustrate the sensitivity of evolutionary path to variations in surface

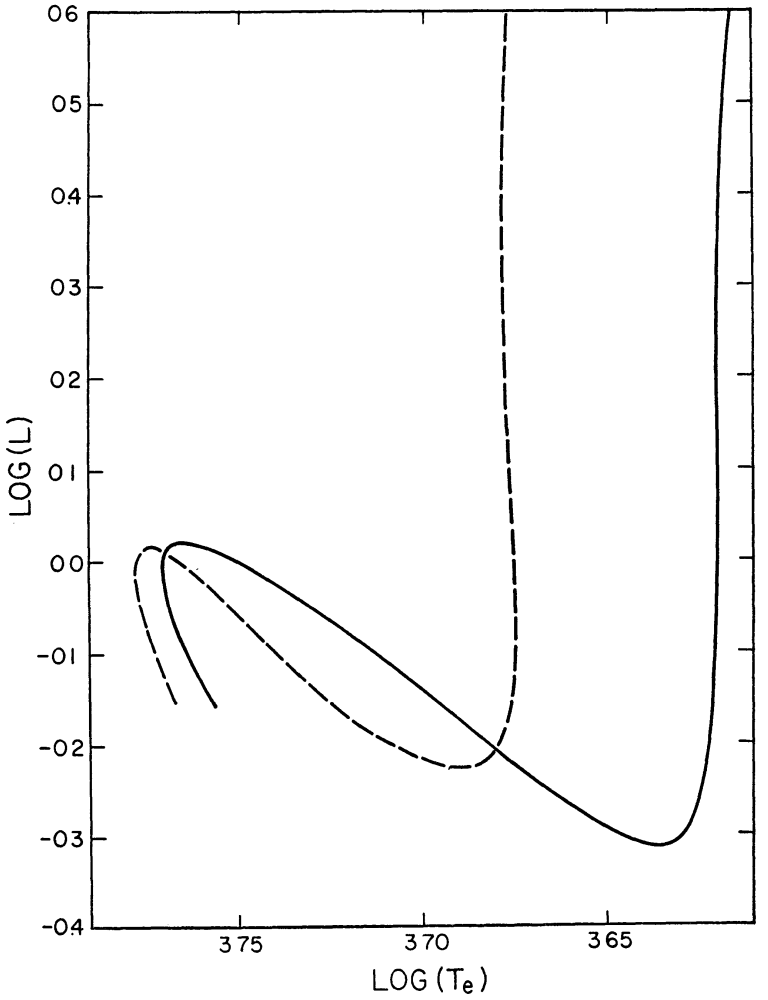

FIG. 1.—Paths in the theoretical Hertzsprung-Russell diagram for $M = M\odot$. Luminosity in units of $L\odot = 3.86 \times 10^{33}$ erg/sec and surface temperature T_e in units of ° K. Solid curve constructed using a mass fraction of metals with 7.5-eV ionization potential, $X_M = 5.4 \times 10^{-5}$. Dashed curve constructed with $X_M = 5.4 \times 10^{-6}$.

opacity, a sequence of 1 $M_\odot$ models has been constructed with the number of metals of low ionization potential reduced by a factor of 10 relative to the number associated with the primary sequence. The dashed curve in Figure 1 describes the resulting path. It is clear that a more careful treatment of surface opacity (not lumping all metals of low ionization potential together as in the present work) will lead to a less vertical track than in the present instance. Further, contributions to opacity by "H_2^-" absorption and Rayleigh scattering may have a non-negligible effect. Uncertainty as to the abundance of elements of low ionization potential relative to one another and relative to hydrogen introduces still further argument against accepting as definitive the present primary track for the very early contraction stages.

A more compelling reason for expressing caution against the literal acceptance of the present model representations of early contraction phases is the high probability of considerable mass loss (Kuhi 1964), perhaps as much as 50 per cent of the star's mass being lost during the low-temperature phase. Finally, in the photospheric layer of the present high-luminosity, low-surface-temperature models, the mean free path of a typical photon is comparable to the temperature scale height. This means, of course, that the standard approximation to radiative transfer, as it is customarily employed in stellar model work, is quite unreliable in the very region where radiative transfer affects most strongly the course of evolution.

Despite the difficulties and uncertainties just described, differential lifetimes obtained for the phase of decreasing luminosity may be accepted in order of magnitude. However, since it is not known at what point a real star first reaches the Hayashi track (Hayashi 1961; Hayashi, Hoshi, and Sugimoto 1962) after dynamic collapse following formation, absolute lifetimes cannot be given.

As the star descends in the H-R diagram, opacities in the deep interior continue to drop with rising interior temperatures until eventually the radiative temperature gradient becomes smaller than the adiabatic temperature gradient in a finite region near the center. A radiative core develops and continues to grow monotonically with time until the flux of energy through the major portion of the star is controlled primarily by an interior opacity which decreases with rising interior temperatures, rather than by a surface opacity which increases with rising surface temperatures—as was the case during the dominantly convective phase of evolution. Luminosity and surface temperature thenceforth grow together until interior temperatures become large enough to fire nuclear reactions near the center.

The details of the transformation from the fully convective to the fully radiative state are made clear in Figure 2. The variation in surface characteristics and in two interior-structure characteristics are given as functions of log (t), time t being measured in seconds from the initial model (log $L \sim 1.2$). Here T_e = surface temperature in units of °K, L = luminosity in units of 3.86×10^{33} erg/sec, R = radius in units of 6.96×10^{10} cm, Q_{RC} = mass fraction through which energy flows by radiation, and $(\rho_c/\bar{\rho})$ = central density over mean density.

As the radiative core grows, matter condenses preferentially toward the center. The change in central concentration may be interpreted as a change in effective polytropic index. Log $(\rho_c/\bar{\rho}) = 0.77815$ corresponds to a polytrope of index 1.5, while log $(\rho_c/\bar{\rho}) = 1.73528$ corresponds to a poytrope of index 3.0 (Eddington 1926). The effective polytropic index thus changes from about 1.5, appropriate to the fully convective state, to slightly above 3.0, appropriate to the fully radiative state with Kramers' opacity (Chandrasekhar 1939). It may be noted that the star spends a considerable portion of its time prior to nuclear burning in a phase of rapidly changing polytropic index. It is just in this phase that the assumption of homologous changes is most inadequate and leads to an underestimate of evolutionary times. Partially for this reason, the time of $\sim 10^7$ years needed to reach the first luminosity minimum at log $(L) \sim -0.316$ and log $(T_e) \sim 3.634$ is considerably larger than that found by Cameron (1962) and by Weymann and

Moore (1963). Another reason for the discrepancy is, however, the fact that the above-cited authors chose initial composition in such a way as to give a main-sequence luminosity larger than that appropriate to the Sun. This choice leads to a higher average luminosity and hence to more rapid evolution. In the present work, the 1 $M_\odot$ model attains the Sun's luminosity after approximately 4.5×10^9 years.

Details of the transition from predominantly gravitational-energy production to predominantly nuclear-energy production are illustrated in Figure 3, where central state variables and central composition parameters are given as functions of log (t). Here T_c = central temperature in 10^{6} ° K, ρ_c = central density in gm/cm^3, X_3 = He^3 abundance by mass at the center, and X_{12} = C^{12} abundance by mass at the center. The scale limits appropriate to each variable in Figure 3 are given in Table 1.

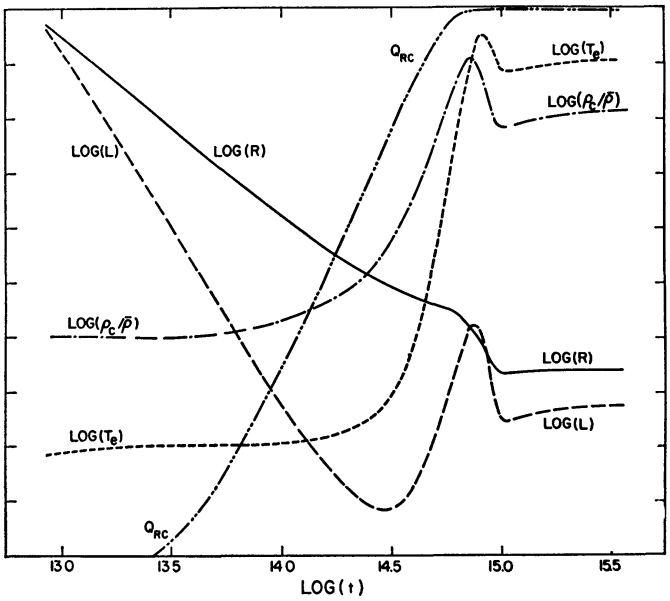

FIG 2.—The variation with time t (in sec) of surface temperature T_e (in units of ° K), luminosity L (in units of 3.86×10^{33} erg/sec), stellar radius R (in units of 6.96×10^{10} cm), central over mean density $\rho_c/\bar{\rho}$, and mass fraction in the radiative core Q_{RC} for a stellar model of mass $M = M_\odot$. Maximum and minimum scale limits correspond to: $3.58 < \log T_e < 3.78$, $-0.4 < \log L < 0.6$, $-0.4 < \log R < 0.6$, $0.0 < \log (\rho_c/\bar{\rho}) < 2.0$, and $0 < Q_{RC} < 1$.

As an illustration of the relationship between Figure 3 and Table 1, consider the curve labeled log T_c in Figure 3. As indicated by the appropriate entries in Table 1 (columns 5 and 6, row 2), the upper and lower bounds of log T_c in Figure 3 are 1.25 and 0.75, respectively. Thus log T_c = 1.15 and T_c = 14.12 ($\times 10^{6}$ ° K) when log (t) = 14.96.

The rapidity with which nuclear-energy production replaces the gravitational source of energy is illustrated by the curve L_g/L in Figure 3 ($0 \leq L_g/L \leq 1$). Precisely defined, L_g is the rate at which the binding energy (= − gravitational potential energy − energy thermal energy) of the star increases with time; L_g/L represent the *net* relative contribution of the gravitational field to the stellar luminosity. The rate at which nuclear sources liberate energy in the star is given by $L_{\rm nuc} = L - L_g$.

It is to be emphasized that, with nuclear sources present, the gravitational field may absorb as well as deliver energy. Hence the actual contribution ($L_g^{\rm out}$) of gravitational energy to the total energy *escaping* the star may be larger than L_g. Similarly, even though $L_{\rm nuc} = L - L_g$ truly represents the rate at which nuclear sources liberate energy *in the star*, the actual contribution ($L_{\rm nuc}^{\rm out}$) of nuclear sources to *escaping* radiation may be considerably less than $L_{\rm nuc}$.

In the present instance, as He^3 builds up appreciably and C^{12} begins to burn rapidly near the center, nuclear energy is supplied near the center faster than it can be carried out. The trapped thermal energy builds up an excess pressure gradient which slows down the rate of contraction, first near the center and then farther and farther out from the center.

As may be seen from the curve of log (ρ_c) versus log (t) in Figure 3, central regions actually begin to expand at log (t) $\sim$ 14.9. In supplying the energy to push central layers out against gravitational forces, nuclear sources now return energy to the gravitational field. L_g thus receives a negative contribution ($-L_g^{abs}$) from the inner expanding regions of the star. The effective contribution of nuclear sources to escaping energy is $L_{nuc}^{out} = L_{nuc} - L_g^{abs}$, whereas the effective contribution of the gravitational field to

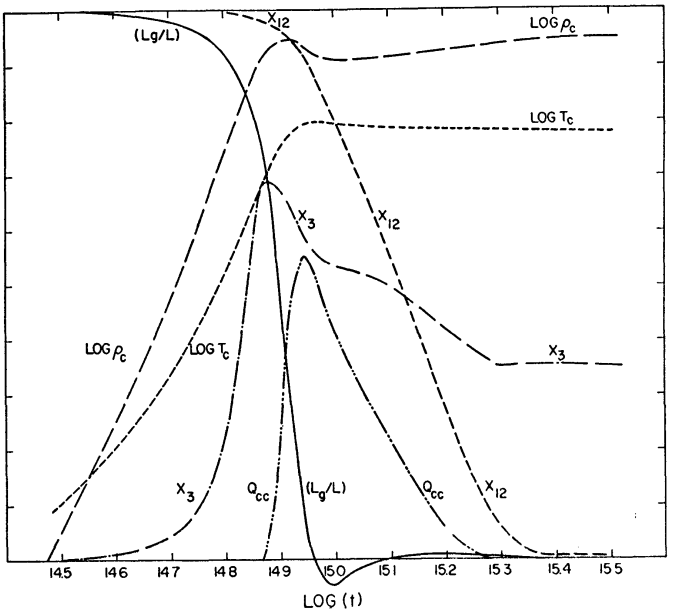

FIG. 3 —The variation with time of He^3 abundance by mass (X_3), C^{12} abundance by mass (X_{12}), central temperature (T_c), central density (ρ_c), mass fraction in a convective core ($Q_{cc} = M_{core}/M_{star}$), and the relative contribution of gravitational energy to the total luminosity (L_g/L). Model mass $M = M\odot$. T_c is in units of 10^6 ° K, and ρ_c is in units of gm/cm^3. Scale limits for all variables but (L_g/L) are listed in Table 1. Within graph boundaries, L_g/L varies from 1 to 0.

TABLE 1

MAXIMUM AND MINIMUM SCALE VALUES

FIGURE	($M/M\odot$)	X_3 (MAX SCALE)	X_{12} (MAX SCALE)	LOG T_c		LOG ρ_c		LOG L		Q_{cc} (MAX SCALE)
				Max Scale	Min Scale	Max Scale	Min Scale	Max Scale	Min. Scale	
11	0 5	$2\ 5\times10^{-3}$		1 00	0 75	2 00	1 00	−0 95	−1 45	1/10
3	1 0	$2\ 0\times10^{-4}$	$3\ 61\times10^{-3}$	1 25	0 75	2 00	1 00			1/5
8	1 5	$5\ 0\times10^{-5}$	$3\ 61\times10^{-3}$	1 30	0 80	2 00	0 75	. .	. .	1/6
13	3 0	$1\ 0\times10^{-5}$	$3\ 61\times10^{-3}$	1 45	0 95	1 70	0 70	+2 15	+1 90	1/3
14	5 0	$2\ 5\times10^{-6}$	$3\ 61\times10^{-3}$	1 50	1 00	1 50	0 50	+3 00	+2 75	1/2
15	9 0	$1\ 0\times10^{-6}$	$3\ 61\times10^{-3}$	1 55	1 05	1 10	0 10	+3 90	+3 65	1/3
16	15 0	$2\ 5\times10^{-7}$	$3\ 61\times10^{-3}$	1 60	1 10	0 90	−0 10	+4 55	+4 30	1/2

escaping energy is $L_g^{out} = L_g + L_g^{abs}$. That this latter amount is supplied by the outer still expanding layers is illustrated in Figure 4.

The distributions of temperature (T), pressure (P), density (ρ), luminosity (L), radius (R), He^3 abundance by mass (X_3), C^{12} abundance by mass (X_{12}), and N^{14} abundance by mass (X_{14}) are given in Figure 4 as functions of mass fraction throughout the stellar interior when log (t) = 14.941. Each variable in Figure 4 is scaled in such a way that the maximum value of that variable in the stellar interior (as defined in Appendix A) has the value unity. Maximum values for the variables are given in Table 2.

The total luminosity of the model described in Figure 4 is $L = 0.911$ ($\times 3.86 \times 10^{33}$ erg/sec). As may be seen from the distribution of luminosity, the still contracting matter in the region beyond mass fraction 0.455, where nuclear-energy sources are negligible, contributes $L_g^{out} = 0.273$ to the total luminosity. Since $L_g/L = 0.0955$ (see Fig. 3), an amount $L_g^{abs} = 0.186$ is used up in pushing out the expanding inner layers. Although nuclear sources liberate energy at the rate $L_{nuc} = L - L_g = 0.824$, only the amount

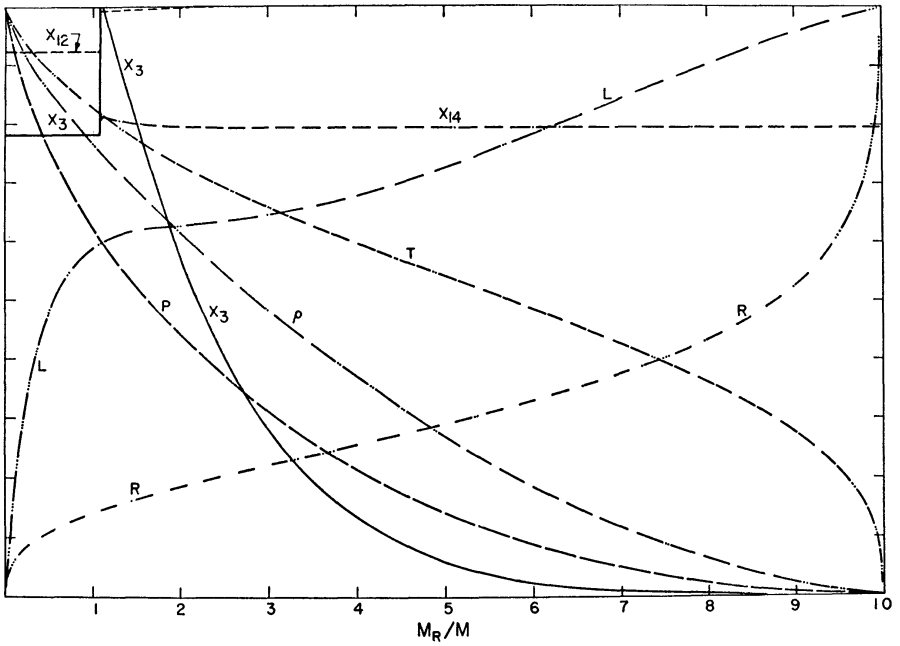

FIG. 4.—The variation with mass fraction of pressure P, temperature (T), density (ρ), luminosity (L), radius (R), He^3 abundance by mass (X_3), C^{12} abundance by mass (X_{12}), and N^{14} abundance by mass (X_{14}). Model mass $M = M\odot$ and log (t) = 14.941. The maximum value of each variable is on the scale of unity. Maximum values in physical units are listed in the first row of Table 2.

TABLE 2

MAXIMUM VALUES FOR DEPENDENT VARIABLES

Figure	P_c (10^{17} dynes/cm^2)	T_c (10^6 ° K)	ρ_c (gm/cm^3)	L_{max} ($3\ 86\times10^{33}$ erg/sec)	R_{max} ($6\ 96\times10^{10}$ cm)	$(X_3)_{max}$	$(X_{12})_{max}$	$(X_{14})_{max}$
4	1 647	14 07	85 59	0 9108	0 8821	$1\ 522\times10^{-4}$	$3\ 61\times10^{-3}$	$1\ 514\times10^{-3}$
5	1 617	13 90	85 15	0 7269	0 8302	$3\ 578\times10^{-4}$	$3\ 61\times10^{-3}$	$4\ 262\times10^{-3}$
9	1 413	16 90	61 51	5 898	1 075	$4\ 861\times10^{-5}$	$3\ 61\times10^{-3}$	$2\ 332\times10^{-3}$
10.	2 208	18 63	87 22	5 411	0 9338	$1\ 513\times10^{-4}$	$3\ 61\times10^{-3}$	$5\ 420\times10^{-3}$

$L_{\text{nuc}}^{\text{out}} = 0.638$ escapes from the star. A true measure of the relative contributions of gravitational and nuclear energy to escaping energy is thus $L_g^{\text{out}}/L_{\text{nuc}}^{\text{out}} = 0.428$, rather than $L_g/L_{\text{nuc}} = 0.106$.

The sudden increase in the central energy supply which brings about the central expansion at log $(t) = 14.9$ leads also to instability against convection in central regions. The mass fraction in the developing convective core is represented as a function of log (t) in Figure 3 by the curve Q_{cc} (from Table 1, $0 \leq Q_{cc} \leq \frac{1}{5}$).

It is not only the high rate of energy generation, but also the high central concentration of the $C^{12}(p, \gamma)N^{13}(\beta^+\nu)C^{13}(p, \gamma)N^{14}$ source which is instrumental in forcing the convective core to develop. The core grows in step with rising interior temperatures and the consequent increase in nuclear energy production by both the $C^{12} \rightarrow N^{14}$ source and the p-p chain sources. The temperature rise is halted when most of the energy leaving the star is supplied by nuclear sources. At its maximum extent, the convective core encompasses 11.06 per cent of the mass of the star.

As C^{12} is depleted near the center and energy production by the p-p chains assumes a more dominant role, the over-all distribution of nuclear sources becomes less pronouncedly peaked toward the center. The mass in the convective core therefore begins to decline and eventually vanishes when the concentration of C^{12} at the center has been reduced to one-tenth of its initial value.

Throughout the growth and decline of the convective core, C^{12} is depleted more rapidly than it is formed. Its abundance at the center drops in a very regular fashion at a rate nearly constant with log (t). Not until after the core disappears does C^{12} come into equilibrium with respect to creating and depleting reactions.

The reason for the curious variations in the abundance of He^3 at the center are somewhat complex and merit attention.

Since the lifetime of a He^3 nucleus against both destruction and creation is long compared to mixing times in the core, He^3 is mixed uniformly throughout the core. As the growing core includes regions at lower and lower temperatures, where He^3 has not been produced as rapidly as at the center, the mixing process begins to drain He^3 from the center, at a rate faster than it can be replenished by creating reactions. With rising central temperatures, however, the average rate of He^3 destruction in the core becomes equal to the average rate of creation; He^3 thereafter remains in average equilibrium. As the core grows, the mean core temperature continues to rise, forcing the equilibrium concentration of He^3 in the core to decrease. The concentration of He^3 at the center thus continues to decrease but at a somewhat faster rate.

Shortly after the core attains its maximum size, interior temperatures decrease asymptotically toward main-sequence values. Now, even though the temperature *distribution* near the center remains nearly constant as the core recedes, the *average temperature* sampled by a typical He^3 nucleus in the core increases. The concentration of He^3 at the center therefore continues to drop but at a still different rate. The final change in the rate of He^3 depletion in the core occurs when interior temperatures cease to drop and the temperature distribution reaches the main-sequence distribution.

It is difficult to determine a criterion by which the main-sequence state may be precisely defined. If one chooses the point at which luminosity reaches its last minimum prior to the major hydrogen-burning stages, then the time to reach the main sequence is $t_{MS} \gtrsim 1.07 \times 10^{15}$ sec $\sim 3.38 \times 10^7$ yr. If one chooses the point at which gravitational and thermal energy sources supply less than 1 per cent (positive contribution) of the star's total energy output, then $t_{MS} \gtrsim 1.6 \times 10^{15}$ sec $\sim 5.06 \times 10^7$ yr.

If the latter definition is more acceptable, then the distributions of state variables and composition parameters in the star when it is almost on the main sequence (log $(t) = 15.199$, $t \sim 5 \times 10^7$ yr) are given in Figure 5 as functions of mass fraction from the stellar center. To the right of the maximum in the curve labeled X_3, He^3 is still building up toward equilibrium values. Between this maximum and the small convective core, He^3 is

in local equilibrium. Within the core, He^3 is in average equilibrium. The discontinuity in the He^3 abundance across the boundary of the convective core points out clearly the difference between assuming average equilibrium abundances and assuming local equilibrium abundances in a convective region. The energy-generation rate via the p-p chain reactions is slightly larger at the center of the core and slightly smaller at the edge of the core than would be the case had local equilibrium abundances been assumed. Since the lifetime of a He^3 nucleus in the convective core is quite large ($t_{1/2} \sim 200$ yr) relative to mixing times in the core ($t_{\text{mix}} \sim$ days), the assumption of average equilibrium values is amply justified.

The near discontinuity in the C^{12} abundance (curve X_{12} in Fig. 5) occurs at the mass fraction which defined the outer edge of the convective core at its maximum extent. C^{12} is still far from equilibrium throughout the star.

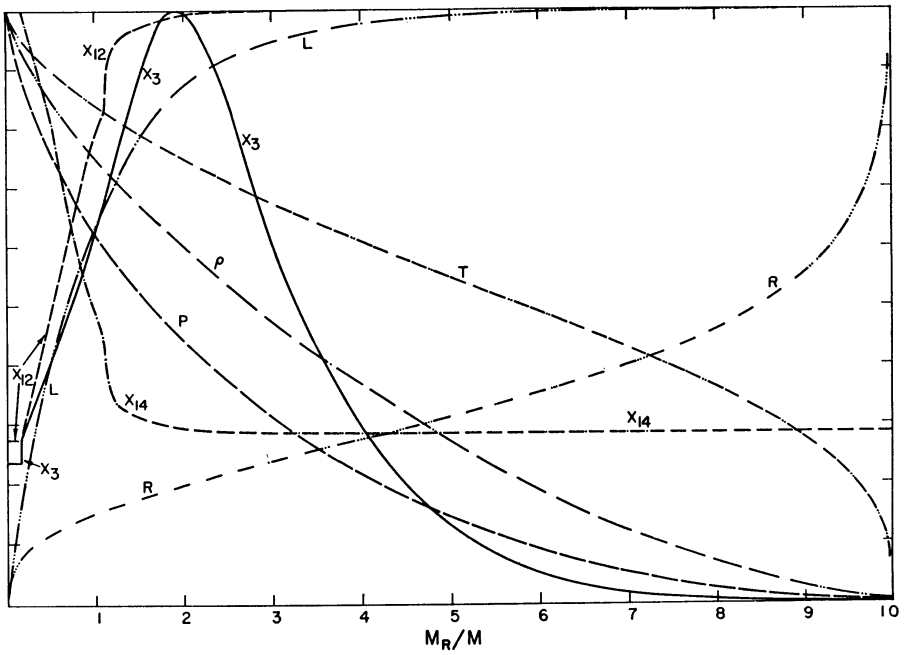

FIG 5.—The variation with mass fraction of the same variables defined under Fig. 4 Model mass $M = M_\odot$ and log $(t) = 15.199$. Maximum values of all variables are listed in the second row of Table 2.

IV. EVOLUTION AT $M = 1.5\ M_\odot$

The evolutionary path of a 1.5 $M_\odot$ model in the H-R diagram is shown in Figures 6 and 17. The variation of central and surface characteristics is shown in Figures 7 and 8. Scale limits for the variables in Figure 8 are given in Table 1. The behavior during the evolutionary phases prior to nuclear burning is identical with that of 1 $M_\odot$ evolution. The initial model, with log $(L) \sim 1.5$, log $T_e \cong 3.61$, is fully convective. A radiative core appears at log $(L) \sim 0.96$ and grows until it encompasses most of the stellar interior (Q_{RC} in Fig. 7). The central condensation, measured by log $(\rho_c/\bar{\rho})$ in Figure 7, increases from a value appropriate to a polytrope of index 1.5 to a value appropriate to a polytrope of index slightly greater than 3.0. As He^3 begins to form rapidly, the nuclear energy released supplements the contribution of gravitational contraction to the total energy output. As C^{12} begins to burn rapidly, almost simultaneously at log $(t) \sim 14.41$ a convective core forms, the rate of central contraction drops sharply, and He^3 comes into equilibrium at the center (see the curves for Q_{cc}, log (ρ_c), and X_3 in Fig. 8).

The sudden increase in the central energy supply brought about by rapid nuclear

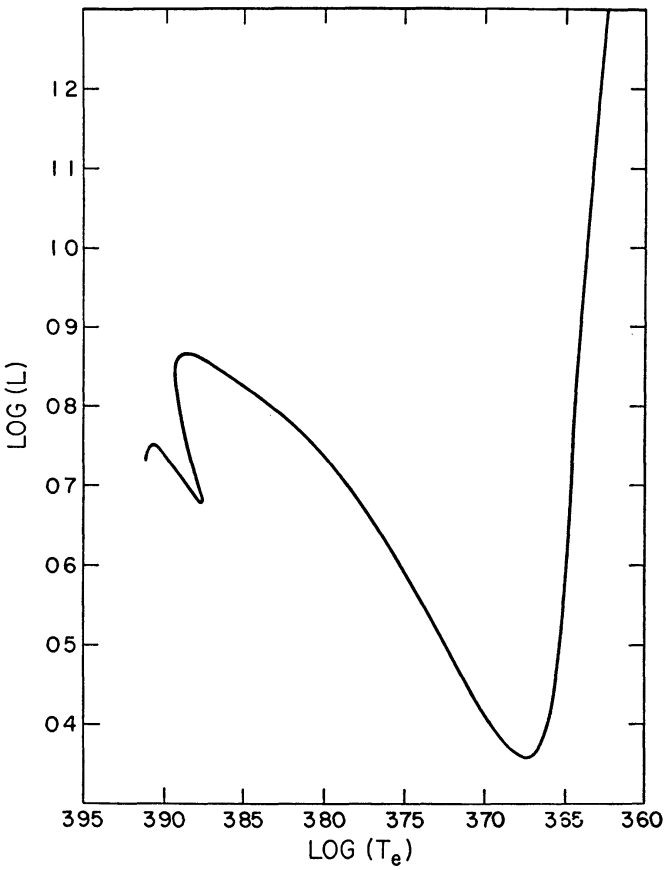

FIG. 6.—The path in the Hertzsprung-Russell diagram for $M = 1.5\ M\odot$. Units of luminosity and surface temperature are the same as in Fig. 1.

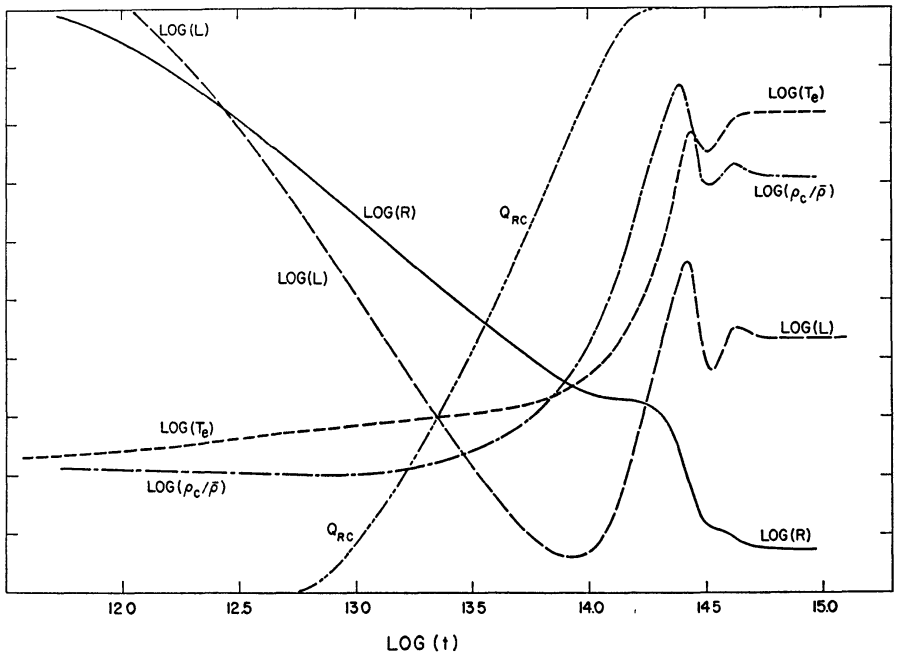

FIG. 7.—The variation with time of the same quantities defined under Fig. 2 for a stellar model with $M = 1.5\ M\odot$. Maximum and minimum scale limits correspond to: $3.5 < \log T_e < 4.0$, $0.3 < \log L < 1.3$, $0.0 < \log R < 1.0$, $0.4 < \log (\rho_c/\bar{\rho}) < 2.4$, and $0 < Q_{RC} < 1$.

burning leads to an overheating and expansion of the inner layers of the star. Luminosity declines as these inner expanding layers not only cease to contribute to the energy flux escaping the star, but blanket the nuclear source by absorbing a large fraction of the nuclear energy produced. As has been demonstrated in the discussion of 1 $M_\odot$ evolution, the fact that the *net* contribution of gravitational energy (measured by L_g/L in Fig. 8) decreases to such small values during this stage is somewhat misleading. The outer still contracting layers continue to contribute an appreciable amount of gravitational energy per second to the energy leaving the star. This is illustrated again in Figure 9 which gives, as a function of mass fraction, the distribution of various parameters through the star at

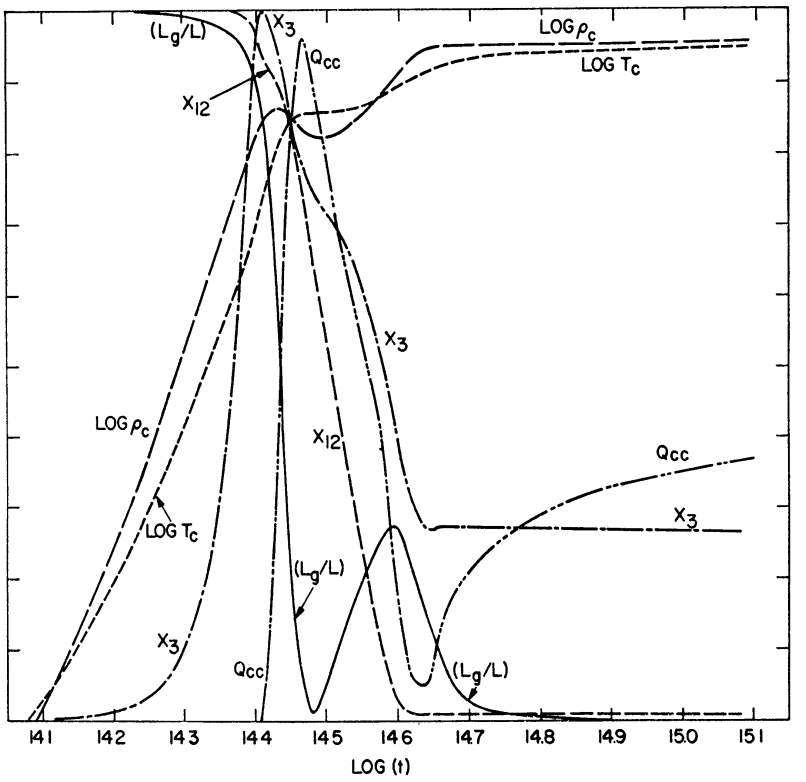

FIG. 8.—The variation with time of the same quantities defined under Fig 3 for $M = 1.5\ M_\odot$ Scale limits for all variables are listed in Table 1.

log $(t) = 14.469$, when the convective core has nearly attained its maximum mass. Maximum values for the variables in Figure 9 are given in Table 2. An examination of the variation of L with mass fraction shows that the contracting matter beyond mass fraction 0.367 contributes 33.5 per cent of the escaping energy, even though the net contribution of gravitational energy is only 3.14 per cent. The expanding layers interior to mass fraction 0.367 absorb 31.4 per cent of the nuclear energy produced per second, allowing nuclear sources to contribute only 66.5 per cent of the energy escaping the star.

As C^{12} decreases, the $C^{12} \rightarrow N^{14}$ source of nuclear energy is reduced in strength relative to the less strongly temperature-dependent p-p chain sources. The convective core therefore diminishes in mass.

A log $(t) \sim 14.49$, C^{12} has been reduced to a sufficient extent that the rate of release of nuclear energy is inadequate to maintain the expansion of the central regions. The flux of energy through the interior, however, is set by the temperature distribution already established. In order to maintain this flux, central regions must again contract

with a consequent increase in the net rate of release of gravitational energy. The layers within and beyond the region of nuclear-energy production no longer blanket the nuclear source which, although diminishing in strength as C^{12} is depleted, now contributes a larger fraction of its output to escaping radiation. After a slight phase lag, nuclear and gravitational sources contribute together to a rising luminosity ($\log (t) \gtrsim 14.505$).

As C^{12} approaches equilibrium, the rising temperatures and densities in the contracting central regions permit the rate of nuclear-energy production to increase again. For the second time, a slight overheating causes the contraction rate to decrease and forces the gravitational source to wane in strength. The luminosity drops slowly down to its main-sequence value.

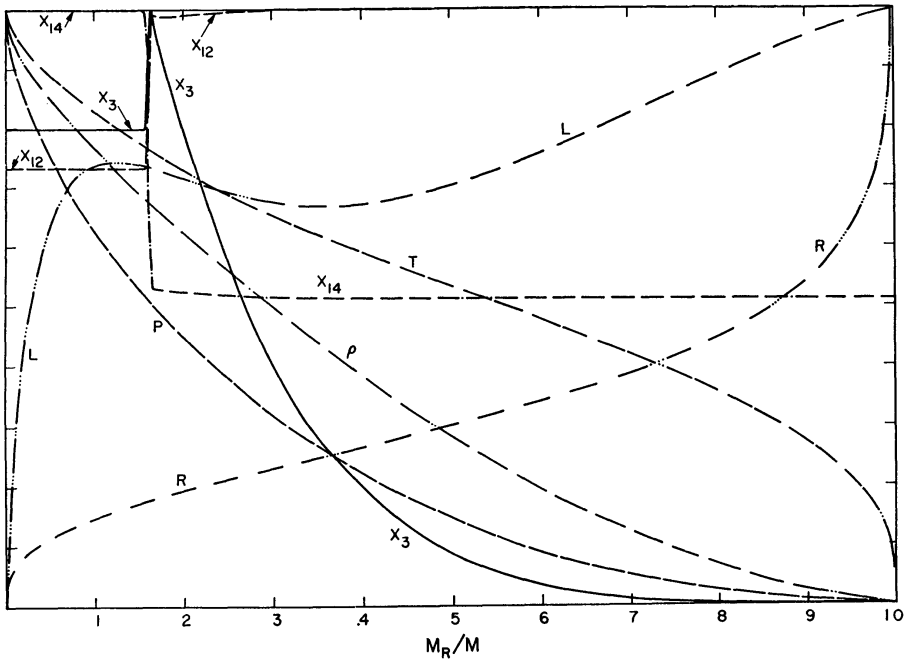

FIG 9.—The variation with mass fraction of variables defined under Fig. 4 for $M = 1\ 5\ M\odot$; $\log (t) = 14.469$. Maximum values of all variables are listed in the third row of Table 2.

During the approach to the main-sequence state and for some time afterward, the rise in central temperatures increases the concentration of nuclear sources near the center (enhances the C-N cycle contribution relative to the *p-p* chain contribution); thus, for a second time, the boundary of the region of convective instability extends to larger and larger mass fraction.

The difference between the present case, in which a strong secondary phase of core contraction follows the depletion of C^{12} below a critical value, and the case of 1 $M\odot$, in which the secondary phase is much less pronounced and does not manifest itself in the H-R diagram, lies in the fact that, relative to the rate at which the *p-p* chain reaction release energy, the rate at which the conversion of C^{12} to N^{14} releases energy is much greater in the 1.5 $M\odot$ star that in the 1 $M\odot$ star. The major conversion of C^{12} to N^{14} occurs in the 1.5 $M\odot$ star at a central temperature of about 17 million degrees, but occurs in the 1 $M\odot$ star at a central temperature of only 14 million degrees. Similarly, the fact that the convective core does not vanish completely, as in the 1 $M\odot$ star, but grows once more following the termination of the secondary phase of gravitational contraction, reflects the greater relative importance of the C-N cycle reactions in the 1.5 $M\odot$ star.

Since the gravitational contribution to the luminosity vanishes as luminosity approaches its final minimum preceding the main hydrogen-burning phase, the point of minimum luminosity (log $(t) \sim 14.9$) may be chosen relatively unambiguously as the main-sequence state. However, the rate at which L approaches this minimum is extremely slow following the termination of the secondary phase of core contraction. For this reason, the *time* to reach the main sequence shall be defined as the time at which L_g/L reaches 0.01 before vanishing. Then log $(t_{MS}) \sim 14.76$ and $t_{MS} \sim 5.75 \times 10^{14}$ sec $\sim 1.82 \times 10^7$ yr.

The distribution versus mass of various characteristics in the star near the main sequence, when log $(t) = 14.798$ and L is within 0.1 per cent of the final minimum, is shown in Figure 10. Maximum values for the variables in Figure 10 are given in Table 2.

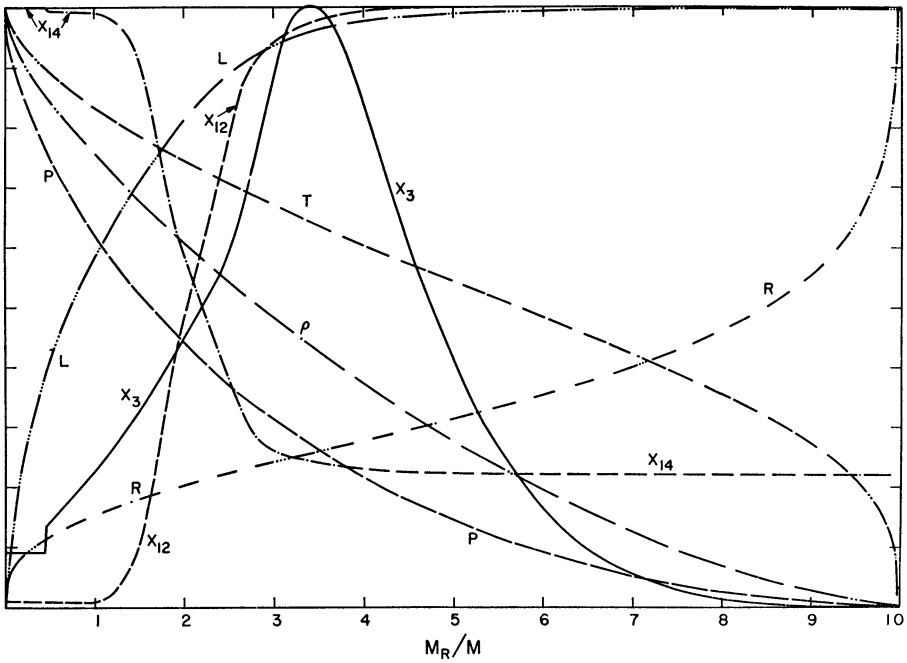

FIG. 10.—The variation with mass fraction of variables defined under Fig. 4 for $M = 1.5\ M_\odot$; log $(t) = 14\ 798$ Maximum values of all variables are listed in the fourth row of Table 2.

Note that the luminosity, and hence the effective energy-generation rate, is a shallower function of mass fraction than in the 1 $M_\odot$ star at the corresponding stage near the main sequence (see Fig. 5). This is a consequence of the fact that, in the 1.5 $M_\odot$ star, the conversion of C^{12} to N^{14} contributes significantly to the energy production at a considerable distance from the center.

It may be noted that, prior to attaining the main-sequence state, some O^{16} has been converted into N^{14} in the convective core. Some hydrogen has been converted into He^4. In fact, when log $(t) = 14.9$ sec, the hydrogen mass fraction at the center has been reduced from 0.708 to 0.704.

V. EVOLUTION AT $M = 0.5\ M_\odot$

The evolutionary path of a 0.5 $M_\odot$ star is shown in Figure 17 (see below).The variation with time of central characteristics and of log (L) is shown in Figure 11. The scale limits for each variable may be found in Table 1.

In this case, the radiative core grows to include at most 66 per cent of the mass of the star (Q_{RC} in Fig. 11). Luminosity therefore does not rise appreciably prior to reaching

the main sequence. Interior temperatures and densities at no time reach high enough values to burn C^{12}. It is solely the energy released in the formation and destruction of He^3 which leads to the decrease in the rate of gravitational contraction. Expansion of central region at log $(t) \sim 15.53$ coincides with the formation and growth of a convective core. It is most interesting that the energy flux contributed by the reactions forming and depleting He^3 is sufficiently strong to maintain convection near the center—contrary to what one might expect on the basis of static main-sequence models.

Luminosity rises between log $(t) \sim 15.8$ and log $(t) \sim 16.4$ even though central densities and temperatures are dropping. This is due both to the diminishing effect of the "expansion blanket" and to the fact that the rate of He^3 production continues to exceed the rate of destruction. He^3 does not reach equilibrium values in the convective core until

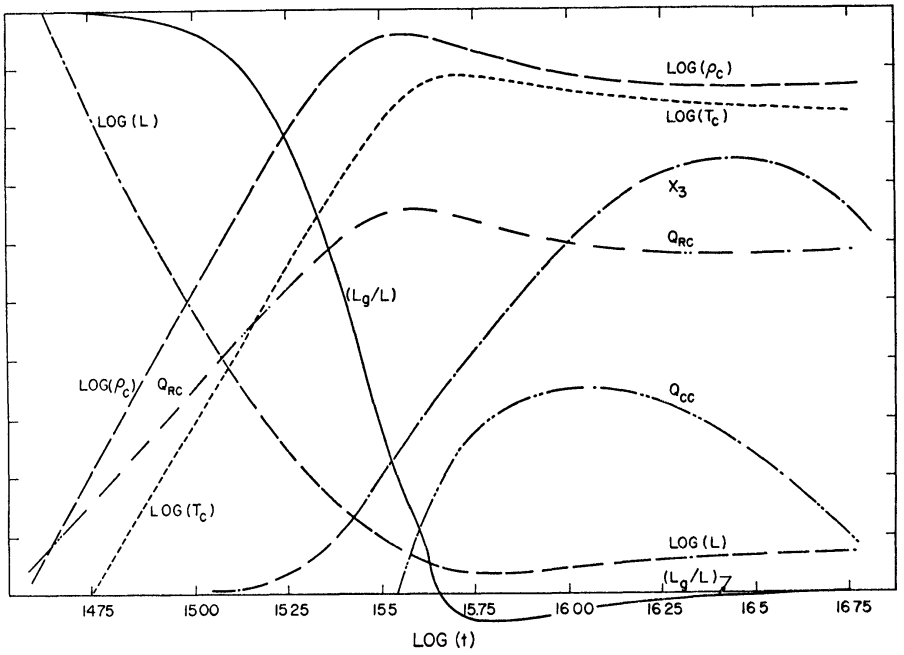

FIG 11 —The variation with time of the quantities defined under Fig 3 and of the variables L and Q_{RC} defined under Fig. 2. Model mass $M = 0\ 5\ M\odot$. Scale limits for all variables but Q_{RC} are listed in Table 1. $0 < Q_{RC} < 1$.

after the core mass has decreased to about three-fourths of its maximum value at log $(t) \sim 16.4$.

Expansion persists considerably beyond the point of minimum luminosity, which occurs when log $(t) \sim 15.8$. This point may not, in a rigorous sense, be defined as the main sequence, since considerable energy is being absorbed by the expanding interior regions $(L_g/L \sim -0.05)$. However, since luminosity changes much more slowly after this point is reached than it changes before this point is reached, the time at which minimum luminosity is achieved may, from a practical standpoint, be called the time to reach main-sequence position. The time required by the 0.5 $M\odot$ star to reach the main sequence is then $t_{MS} \sim 6 \times 10^{15}$ sec $\sim 2 \times 10^8$ yr.

Interpolating by means of a smooth curve drawn through t_{MS} for $(M/M\odot = 0.5, 1.0,$ and 1.5, one finds a time $t_{MS} \sim 1.4 \times 10^8$ yr for an 0.6 $M\odot$ star to reach the main sequence. This agrees quite well with the time $t_{MS} \sim 1.43 \times 10^8$ yr found by Hayashi *et al.* (1962) for an 0.6 $M\odot$ star. The agreement is due in part to the fact that the homology assumption employed by Hayashi *et al.* (1962) is approximately valid over a much greater segment of the evolutionary path than is the case for more massive stars.

VI. EVOLUTION AT $(M/M_\odot) = 3, 5, 8,$ AND 15

Evolutionary paths for $M/M_\odot = 3, 5, 9,$ and 15 are shown in Figure 12. The variation with time of surface and central characteristics for $M = 3\ M_\odot$ is given in Figures 12 and 13. Figures 14–16 describe the variation with time of central characteristics and of log (L) for $M/M_\odot = 5, 9,$ and 15, respectively. Scale limits for the variables in Figures 13–16 are found in Table 1.

For $M \leq 5\ M_\odot$, the strength of the secondary phase of gravitational contraction increases with increasing stellar mass, as energy generation by the p-p chain reactions becomes less effective as a buffer between the C^{12} depletion stage and the main C-N cycle burning stage.

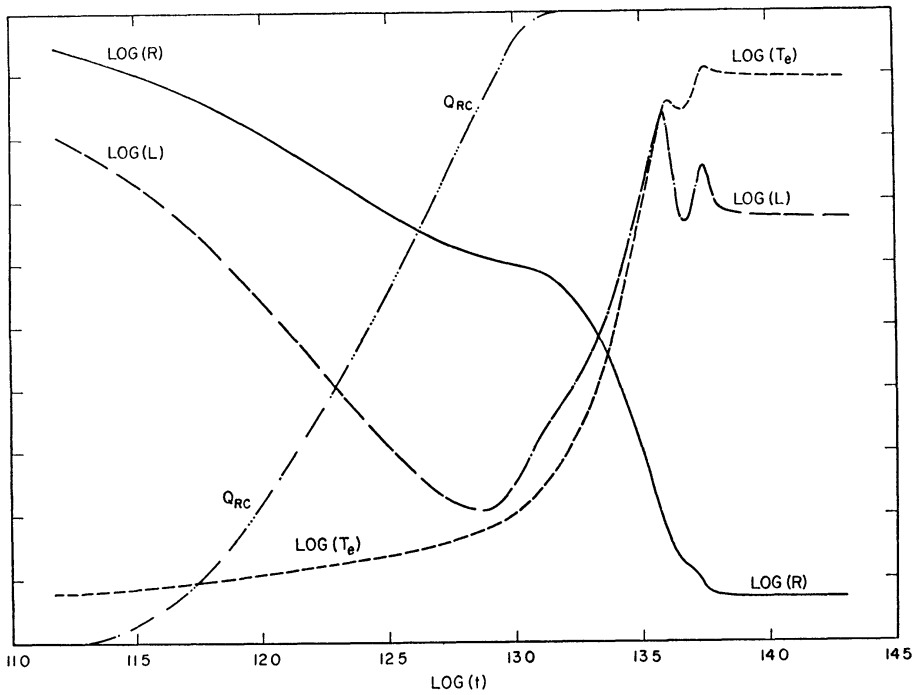

FIG 12.—The variation with time of the same quantities defined under Fig. 2 for a stellar model with $M = 3\ 0\ M_\odot$. Maximum and minimum scale limits satisfy: 3 575 < log (T_e) < 4 20, 1.30 < log (L) < 2 30, 0 15 < log R < 1.40, and 0 < Q_{RC} < 1.

Between 5 $M_\odot$ and 15 $M_\odot$, the transition from the stage of pure gravitational contraction to the main-sequence stage of pure nuclear burning becomes increasingly smoother with increasing stellar mass: the fractional drop in luminosity between the onset of C^{12} burning and the secondary phase of central gravitational contraction becomes less pronounced; the strength of the secondary phase of gravitational contraction diminishes; the minimum mass in the convective core becomes larger both relative to the core mass at its height during the C^{12} depletion stage and relative to the core mass during the main-sequence stage; the extent of the first expansion during the C^{12} depletion stage as well as the extent of expansion following the secondary phase of rapid contraction decreases (in fact, for $M = 15\ M_\odot$, central regions do not expand at all following C^{12} depletion, but continue to contract).

A number of effects contribute to this increasing smoothness. The lifetime of a C^{12} nucleus against proton capture decreases relative to the lifetime of an N^{14} nucleus against proton capture; the transition from the $C^{12} \rightarrow N^{14}$ source of energy to the full C-N cycle source of energy becomes less abrupt. With increasing stellar mass, radiation pressure be-

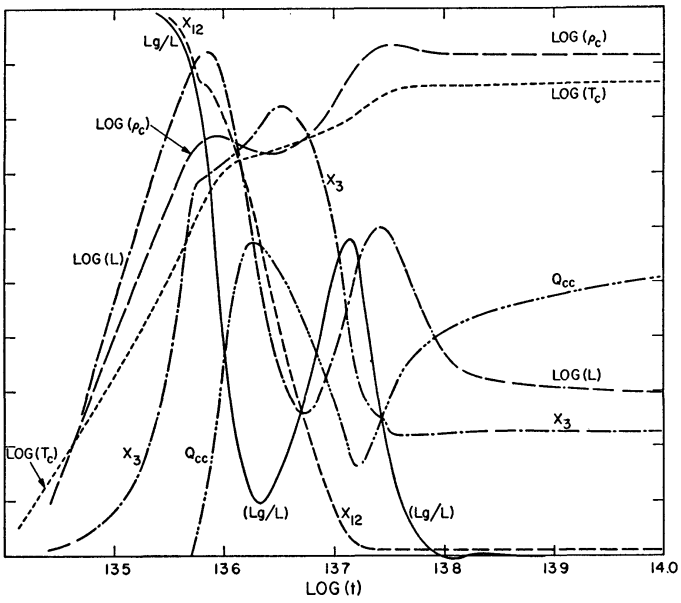

FIG 13.—The variation with time of the same quantities defined under Fig 3 and of stellar luminosity for $M = 3.0\ M\odot$. Scale limits for all variables are listed in Table 1.

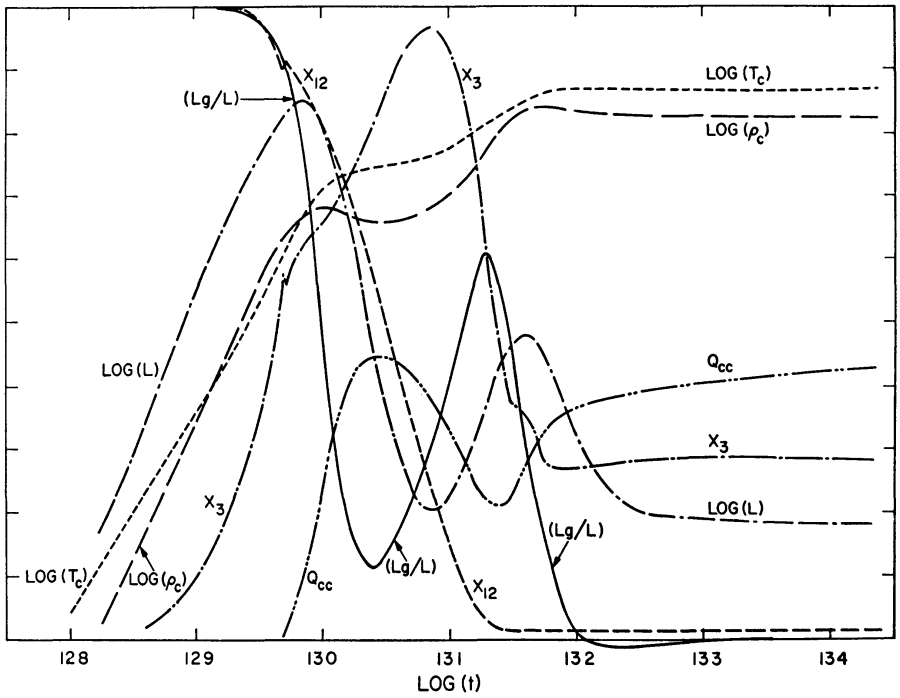

FIG. 14.—The variation with time of the same quantities defined under Fig 3 and of stellar luminosity for $M = 5.0\ M\odot$. Scale limits for all variables are listed in Table 1.

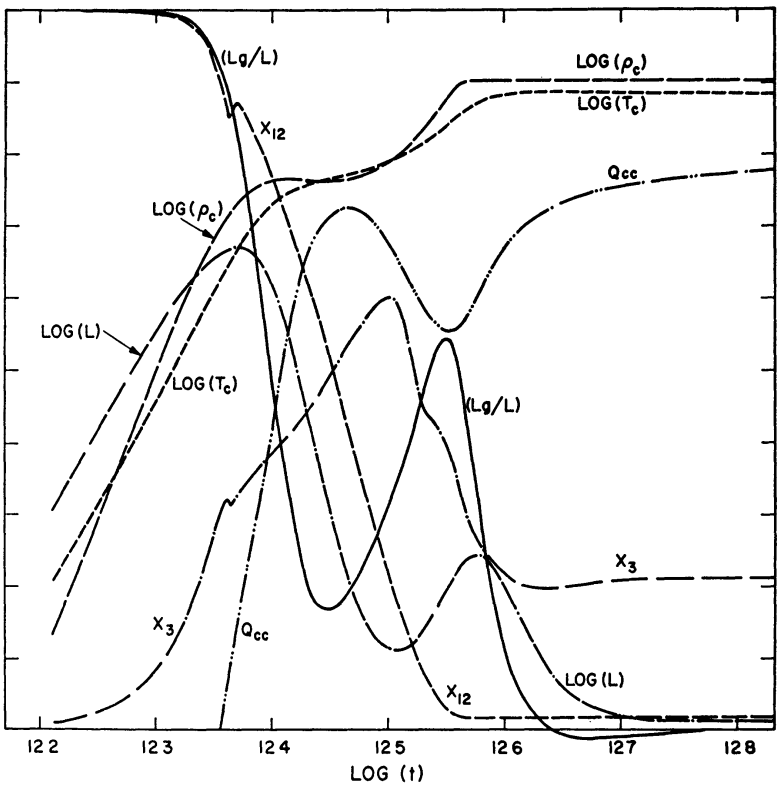

FIG. 15 —The variation with time of the same quantities defined under Fig 3 and of stellar luminosity for $M = 9.0\ M\odot$. Scale limits for all variables are listed in Table 1.

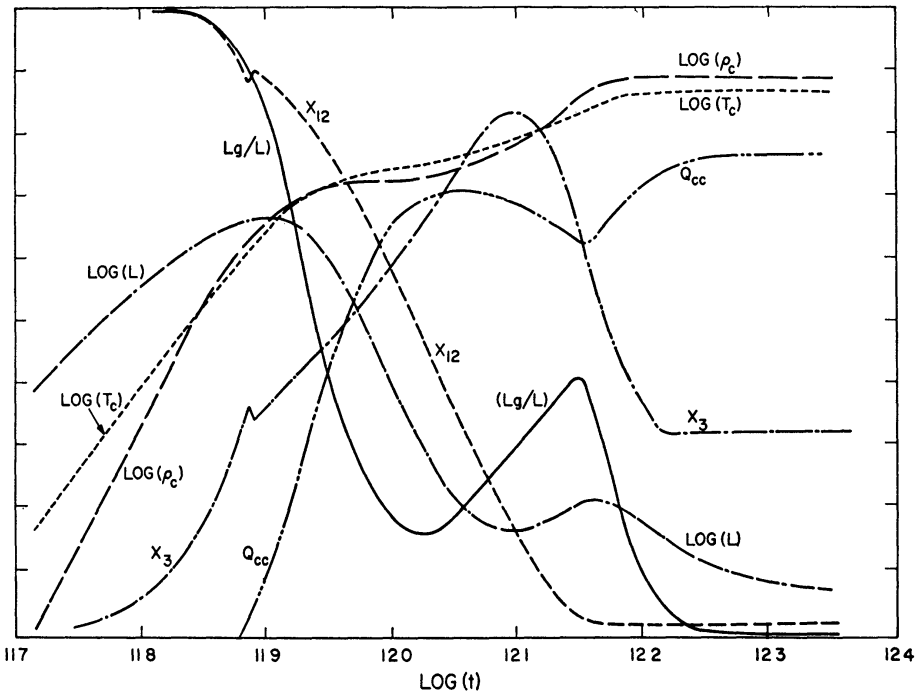

FIG. 16 —The variation with time of the same quantities defined under Fig 3 and of stellar luminosity for $M = 15\ 0\ M\odot$. Scale limits for all variables are listed in Table 1.

comes a larger fraction of the total pressure and electron scattering replaces free-free and bound-free absorption as the main contributor to interior opacity; the adiabatic temperature gradient in the convective core and the radiative gradient outside of this core approach one another more closely so that the changes in structure accompanying variations in the core mass become less radical.

As in the case of $M = 1.5\ M_{\odot}$, the point at which luminosity attains its final minimum, before increasing during the main hydrogen-burning stages, may be defined as the

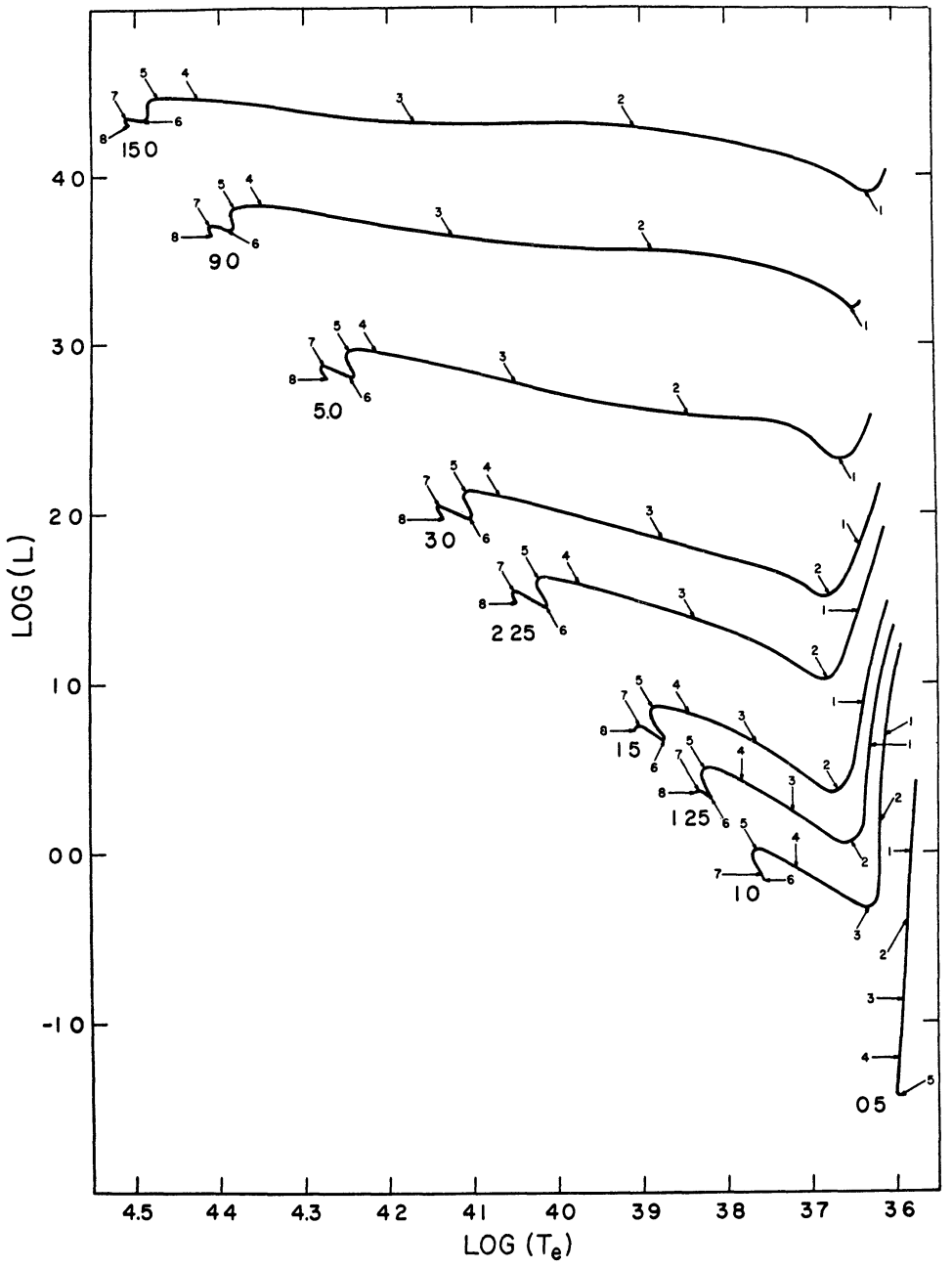

FIG. 17.—Paths in the Hertzsprung-Russell diagram for models of mass ($M/M_{\odot}$) = 0.5, 1.0, 1.25, 1.5, 2.25, 3 0, 5.0, 9.0, and 15.0. Units of luminosity and surface temperature are the same as those in Fig. 1

TABLE 3

EVOLUTIONARY LIFETIMES

POINT	$(M/M_\odot)$								
	15.0	9.0	5.0	3.0	2.25	1.5	1.25	1.0	0.5
1.	6.740×10^{2}	1.443×10^{3}	2.936×10^{4}	$3\ 420\times10^{4}$	7.862×10^{4}	2.347×10^{5}	4.508×10^{5}	1.189×10^{5}	$3\ 195\times10^{5}$
2. .	$3\ 766\times10^{3}$	1.473×10^{4}	1.069×10^{5}	2.078×10^{5}	5.940×10^{5}	2.363×10^{6}	3.957×10^{6}	1.058×10^{6}	1.786×10^{6}
3 .	9.350×10^{3}	$3\ 645\times10^{4}$	2.001×10^{5}	$7\ 633\times10^{5}$	1.883×10^{6}	5.801×10^{6}	8.800×10^{6}	8.910×10^{6}	8.711×10^{6}
4. .	2.203×10^{4}	6.987×10^{4}	2.860×10^{5}	1.135×10^{6}	2.505×10^{6}	7.584×10^{6}	1.155×10^{7}	1.821×10^{7}	$3\ 092\times10^{7}$
5. . . .	2.657×10^{4}	7.922×10^{4}	$3\ 137\times10^{4}$	1.250×10^{6}	2.818×10^{6}	8.620×10^{6}	1.404×10^{7}	2.529×10^{7}	1.550×10^{8}
6. . .	3.984×10^{4}	1.019×10^{5}	3.880×10^{5}	1.465×10^{6}	3.319×10^{6}	1.043×10^{7}	$1\ 755\times10^{7}$	$3\ 418\times10^{7}$	
7. . .	4.585×10^{4}	1.195×10^{5}	4.559×10^{5}	1.741×10^{6}	$3\ 993\times10^{6}$	1.339×10^{7}	2.796×10^{7}	$5\ 016\times10^{7}$	
8.	6.170×10^{4}	1.505×10^{5}	$5\ 759\times10^{5}$	2.514×10^{6}	5.855×10^{6}	1.821×10^{7}	2.954×10^{7}		

main sequence. In this state, the hydrogen mass fraction at the center has been reduced, for all masses in the range $3 \leq M/M_\odot \leq 15$, from its initial value of 0.708 to about 0.704. The time to reach the main sequence shall be taken as the time for luminosity to decrease to within 1 per cent of its final minimum value. With this choice, one finds log (t_{MS}) = 13.90, 13.26, 12.68, and 12.29 for $(M/M_\odot)$ = 3, 5, 9, and 15, respectively. The corresponding times ($t_{MS} = 2.514 \times 10^6$ yr, 5.759×10^5 yr, 1.505×10^5 yr, and 6.170×10^4 yr) are about 1.6 times larger than times given by the classical expression $t_{MS}' = 5 \times 10^7\ (M/M_\odot)(L_\odot/L)$ years (Schwarzschild 1958), obtained on the basis of a Kramer's opacity, and about 3.2 times larger than times given by a similar expression based on an electron-scattering opacity. The values of $t_{MS} = 2.954 \times 10^7$ yr, 1.821×10^7 yr, and 5.855×10^6 yr obtained for $(M/M_\odot)$ = 1.25, 1.5, and 2.25 (paths for $M = 1.25\ M_\odot$ and $M = 2.25\ M_\odot$ are shown in Fig. 17) are about twice as large as those found by Henyey *et al.* (1955). The longer times found here are due, in large part, to the time spent by the star in the C^{12} depletion stage.

VII. SUMMARY OF LIFETIMES

For ease of comparison, the times for model stars of various masses to reach successive points along their evolutionary paths in the Hertzsprung-Russell diagram are given in Table 3. Times are measured in years from the initial model in each case and numbers correspond to the points designated in Figure 17. The last entry in each case corresponds to the main-sequence stage as defined in previous sections.

Special thanks are due to Professor William A. Fowler, the Office of the Naval Research, the National Aeronautics and Space Administration, and the entire staff of the California Institute of Technology computing center for making possible the work described in this paper.

APPENDIX A

CALCULATIONAL TECHNIQUES

The procedure used in obtaining evolutionary models is a modification of the method described by Henyey *et al.* (1964). The interior of the star is divided into shells of mass $\Delta M_i = M_i - M_{i-1}$, where M_i represents the mass interior to the ith shell. Pressure (P_i), temperature (T_i), luminosity (L_i), radius (R_i), and composition parameters $(X_i(j))$ are defined at shell boundaries. Density $(\rho_{i-1/2})$, opacity $(\kappa_{i-1/2})$, and the rate of energy generation $(\epsilon_{i-1/2})$ are defined at shell interstices as functions of $P_{i-1/2} = (P_i + P_{i-1})/2$, $T_{i-1/2} = (T_i + T_{i-1/})/2$, and the quantities $X_{i-1/2}(j) = (X_i(j) + X_{i-1}(j))/2$.

The appropriate difference equations to be satisfied at all points in the interior are cast in the form

$$C_1(i) = \ln\left[\frac{P_i - P_{i-1}}{R_i - R_{i-1}} \frac{R^2_{i-1/2}}{GM_{i-1/2}\rho_{i-1/2}}\right] = \ln A_1(i),$$

$$C_2(i) = \ln\left[\frac{4\pi R^2_{i-1/2}(R_i - R_{i-1})\,\rho_{i-1/2}}{\Delta M_i}\right] = \ln A_2(i),$$

$$C_3(i) = \ln\left[\frac{L_i - L_{i-1}}{\epsilon_{i-1/2}\Delta M_i}\right] = \ln A_3(i), \tag{A1}$$

$$C_4(i) = \ln\left[\frac{(T_i - T_{i-1})P_{i-1/2}}{(P_i - P_{i-1})T_{i-1/2}} \frac{1}{(V)_{i-1/2}}\right] = \ln A_4(i),$$

where $V_{i-1/2} = [d(\ln T)/d(\ln P)]_{i-1/2}^{\text{adiabatic}}$ or $V_{i-1/2} = (\frac{3}{16}\pi acG)(\kappa PL/MT^4)_{i-1/2}$, whichever is smaller, and $M_{i-1/2} = (M_i + M_{i-1})/2$.

Variables at the outer boundary of the last interior shell are constrained to match the values of these same variables at the base of an envelope constructed by integration from the stellar surface inward. The physical properties of envelopes are described by Iben (1963*a*).

Iterations on equations (A1) are performed until the quantities $A_m(i)$ reach the value 1 to the desired accuracy (usually one part in ten thousand). Each iteration involves the solution of the linear perturbation equations

$$C_m(i) + \delta C_m(i) = C_m(i) + \sum_{k=1}^{4} \frac{\partial C_m(i)}{\partial \ln Q_i(k)} \delta \ln Q_i(k) + \sum_{k=1}^{4} \frac{\partial C_m(i)}{\partial \ln Q_{i-1}(k)} \delta \ln Q_{i-1}(k) = 0 \tag{A2}$$

for the $\delta \ln Q_i(k)$ and the $\delta \ln Q_{i-1}(k)$. Here, $Q_i(k) = P_i$, T_i, L_i, and R_i.

In many instances, the differences which appear in equations (1) between two quantities computed at shell boundaries are many orders of magnitude smaller than the quantities themselves. To avoid round-off errors and to achieve convergence, it has been found necessary to calculate and preserve these differences explicitly. For example, let the difference between temperatures at two adjacent shell boundaries be $\Delta T_i = T_i - T_{i-1}$ prior to an iteration. After a solution of the perturbation equations (A2), this difference becomes $\Delta T_i' = \Delta T_i + [T_i\ (\delta \ln T_i) - T_{i-1}\ (\delta \ln T_{i-1})]$. The alternate choice $\Delta T_i'' = T_i(1 + \delta \ln T_i) - T_{i-1}(1 + \delta \ln T_{i-1}) = T_i' - T_{i-1}'$, leads in some instances ($\Delta T_i / T_{i-1/2} <<< 1$) to significant errors and lack of convergence.

Prior to every time step, mass shells are either merged or subdivided into an integral number of equal-mass shells satisfying the criteria

$$\begin{aligned} &|(Q_i^n(k) - Q_{i-1}^n(k))/Q_{i-1}^n(k)| \leq \delta(k), \qquad (k = 1, 4), \\ &|L_i^n - L_{i-1}^n| \leq 0.05\, L_{\max}^n, \\ &|X_i^n(j) - X_{i-1}^n(j)| \leq \lambda(j), \ (j = 1, \text{number of composition parameters}), \end{aligned} \tag{A3}$$

where $L_{\max}^n$ is the maximum value of the luminosity in the star at time t^n, and $\delta(k)$ and $\lambda(j)$ are varied according to the circumstances. Commonly used values of the $\delta(k)$ lie between 0.05 and 0.25. In the case of hydrogen, $\lambda(j) = \lambda(1)$ is usually chosen as 0.01 to 0.015. For less abundant elements, the $\lambda(j)$ are usually chosen in such a way that $|X_i(j) - X_{i-1}(j)| \leq 0.05\,(X_i'(j))_{\max}$. One further restriction is placed on shell size. In a region, δM, centered on a radiative-convective zone-boundary, $\Delta M_i \leq 0.05 \times$ (mass of the convective zone). The region δM satisfies the equality $\delta M = 0.2 \times$ (mass of convective zone).

As a preliminary step in obtaining a trial solution for a time step $\Delta t = t^{n+1} - t^n$, the quantities

$$\sigma_i(k) = (\ln Q_i^n(k) - \ln Q_i^{n-1}(k))/(t^n - t^{n-1}) \tag{A4}$$

are formed. Letting σ be the smallest of the quantities $(\sigma_i(k))$, the time step is first chosen as

$$\Delta t = t^{n+1} - t^n = \mu^n/\sigma, \tag{A5}$$

where μ^n is a predetermined constant. Trial values of all quantities Q_i^{n+1} are found from

$$\ln Q_i^{n+1}(k) = \ln Q_i^n(k) + \sigma_i(k)\Delta t. \tag{A6}$$

The quantity μ^n is usually taken between 0.05 and 0.20, but is varied at different phases of the evolution in such a way that the number of iterations needed to achieve a model multiplied by the computer time required per iteration attains an optimal value.

In some cases, it is found that $(P_i^{n+1} - P_{i-1}^{n+1}) > 0$ or that $R_i^{n+1} - R_{i-1}^{n+1}) < 0$ (i increases

from center to surface). The time step is then reduced until guessed values of P_i decrease monotonically outward and guessed values of R_i increase monotonically outward.

For a given time step, convergence to the desired accuracy cannot always be obtained. The time step is then successively halved until convergence is achieved.

In regions stable against convection, a first choice for the composition parameters appropriate to a new trial model is obtained from the properties of the last completed model via the equations

$$(X_i^{n+1}(j))' = X_i^n(j) + \frac{dX_i^n(j)}{dt}\Delta t. \tag{A7}$$

The final choice is obtained by calculating composition derivatives at time $t^{n+1/2}$ via the equations

$$X_i^{n+1}(j) = X_i^n(j) + \frac{dX_i^{n+1/2}(j)}{dt}\Delta t, \tag{A8}$$

where $X_i^{n+1/2}(j) = [X_i^n(j) + (X_i^{n+1}(j))']/2$, $T_i^{n+1/2} = (T_i^n + T_i^{n+1})/2$, and so forth. In this way, time steps need not be reduced prohibitively during phases of rapid composition changes.

Mathematical instabilities associated with the change in the position of convective-radiative zone-boundaries are avoided by demanding that the distribution of composition parameters as a function of mass is fixed during the course of iteration. Only *after* iterations have been completed is mixing allowed to occur. If, at all points within a convective region, the rate at which a significant change in a particular nuclear species occurs is small relative to the rate of mixing within this region, the mean value of the associated composition parameter is found from

$$\bar{X}^n(j) = (\Sigma X_{i-1/2}^n(j)\Delta M_i)/\Delta M_{\text{convective region}}, \tag{A9}$$

where the summation extends over the convective region. At all points in the convective region, one then sets $X_i^n(j) = \bar{X}^n(j)$ and computes values for $\bar{X}^{n+1}(j)$ in the same way as before, using the mean rates,

$$\frac{d\bar{X}(j)}{dt} = \left(\sum_i \frac{dX_i^n(j)}{dt}\Delta M_i\right) \Big/ \Delta M_{\text{convective region}}. \tag{A10}$$

Special care must be taken in calculating the change in a nuclear species when the time step Δt, chosen on the basis of structural changes, is comparable to the time required for this nuclear species to reach equilibrium with respect to supplying and depleting nuclear reactions. Let $\delta t_i(j)$ be defined as the time for a particular species to reach equilibrium in mass shell i. If $\delta t_i(j) > \Delta t$, changes in $X_i(j)$ may be calculated explicitly with the derivative $dX_i(j)/dt$. If $\delta t_i(j) < \Delta t$, then equilibrium abundances for $X_i(j)$ are to be adopted and changes based on the time derivatives of $X_i(j)$ are to be avoided. If this procedure is not followed, spurious oscillations are the result.

In the present application, C^{12} and O^{16} are depleted toward equilibrium values and He^3 is built up to equilibrium values during evolution. On switching from a derivative calculation of C^{12} and O^{16} changes to an equilibrium calculation, one must be careful to conserve the total number of C^{12}, N^{14}, and O^{16} nuclei. Appropriate conservation among the elements H^1, He^3, and He^4 must also be maintained when He^3 approaches equilibrium values.

APPENDIX B

NUCLEAR-TRANSFORMATION RATES AND NUCLEAR AND GRAVITATIONAL ENERGY-GENERATION RATES

1. It is convenient to express the rate at which two nuclear species, i and j, react in terms of the quantities

$$r_{ij} = (\rho/T^{2/3})X_iX_j \exp(A_{ij} - B_{ij}/T_6^{1/3} + S_{ij}), \tag{B1}$$

where X_i and X_j are the mass fractions of elments i and j and the S_{ij} are appropriate screening factors. With density in gm/cm^3 and temperature in 10^6 ° K, the quantities A_{ij} and B_{ij} are given in the third and fourth columns of Table 4. Zero-energy center-of-mass cross-section factors are essentially the same as those given by Parker, Bahcall, and Fowler (1964), except that the center-of-mass cross-section factor for the $He^3(\alpha, \gamma)Be^7$ reaction is chosen from the raw data of Parker (1963) as 0.6 keV barns. Only first-order terms from the integration over the Maxwell velocity distribution are retained. During all stages in all masses discussed in this paper, the conditions for the validity of Salpeter's (1954) weak screening factors are met. The appropriate screening factors are given in the fifth column of Table 4 in terms of

$$S_0 = 0.752(\rho/T^3)^{1/2}\left(X_1 + \tfrac{4}{3}X_3 + X_4 + 3X_{12} + 3.5X_{14} + 4X_{16} + \frac{1}{\mu_e}\right)^{1/2}, \quad \text{(B2)}$$

where $1/\mu_e = (1 + X_1)/2 + X_3/6$.

TABLE 4

REACTION RATE AND ENERGY-GENERATION RATE PARAMETERS

Reacting Elements	i, j	A_{ij}	B_{ij}	S_{ij}/S_0	$\mathfrak{A}_i = M_i/M_H$	$10^5 E_{ij}$
H^1, H^1	1, 1	25 3511	33 8077	1/4	1	1 07018
He^3, He^3	3, 3	79 8293	122 737	1	2 99262	2 05865
He^4, He^3	4, 3	72 5151	128 266	1	3 97154	0 253126
C^{12}, H^1	12, 1	73 6498	136 913	3/2	11 9069	1 76066
N^{14}, H^1	14, 1	74 3562	152 299	7/4	13 8944	2 24988
O^{16}, H^1	16, 1	75 4758	166 945	2	15 8708	0 568731

The "lifetime" of element i against destruction by element j may be defined as the reciprocal of

$$\left|\frac{1}{X_i}\frac{dX_i}{dt}\right|_j = M_i r_{ij}/X_i, \quad \text{(B3)}$$

where M_i is the mass of the *neutral* atom i in grams. Appropriate masses relative to the mass, M_H, of the hydrogen *atom* are given by the quantities $\mathfrak{A}_i$'s in the sixth column of Table 4. The total rates at which the X_i's change with time are given by

$$\begin{aligned}
\frac{dX_1}{dt} &= M_H[(-3r_{11} + 2r_{33} - r_{34}) - 2(r_{112} + r_{114} + r_{116})], \\
\frac{dX_3}{at} &= M_3(r_{11} - 2r_{33} - r_{34}), \\
\frac{dX_4}{dt} &= M_4[(r_{33} + r_{34}) + (0.999486r_{114} + r_{116})], \\
\frac{dX_{12}}{dt} &= M_{12}(-r_{112} + 0.999486r_{114}), \\
\frac{dX_{14}}{dt} &= M_{14}(-r_{114} + r_{112} + r_{116}), \\
\frac{dX_{16}}{dt} &= M_{16}(0.000514r_{114} - r_{116}).
\end{aligned} \quad \text{(B4)}$$

For convenience, it has been assumed (see Caughlan and Fowler 1964) that, under all conditions, the $N^{15}(p, \gamma)O^{16}$ reaction rate is 0.000514 times as frequent as the $N^{15}(p, \alpha)C^{12}$ reaction rate.

The energy liberated as a result of the fusion of elements i and j is given in erg/reaction by the quantities E_{ij} in the seventh column of Table 4. The energy from the entire sequence $C^{12}(p, \gamma)N^{13}(e^+ \nu)C^{13}(p, \gamma)N^{14}$ is included in E_{112}; energy from the sequence $N^{14}(p, \gamma)O^{15}(e^+ \nu)N^{15}(p, \alpha)C^{12}$ is included in E_{114}; and energy from the sequence $O^{16}(p, \gamma)F^{17}(e^+ \nu)O^{17}(p, \alpha)N^{14}$ is included in E_{116}.

The total nuclear-energy generation rate in erg/gm is

$$\epsilon_{\text{nuc}} = \Sigma E_{ij} r_{ij} , \tag{B5}$$

with the stipulation that E_{34} be replaced by

$$E_{34}' = E_{34} + (\gamma E_{17} + E_{e7})/(1 + \gamma) , \tag{B6}$$

where $E_{17} = 1.73663 \times 10^{-5}$ erg/reaction, $E_{e7} = 2.78598 \times 10^{-5}$ erg/reaction, and

$$\gamma = (0.091179\, X_1 \mu_e / T_6^{1/6}) \exp (39.1440 - 102.639/T_6^{1/3} + S_0) \tag{B7}$$

gives the rate at which Be^7 captures protons relative to the rate at which it captures electrons. The Be^7 electron capture rate is that given by Bahcall (1962) and the center-of-mass cross-section factor for the Be^7 proton capture is that found by Kavanagh (1958).

2. The total energy liberated per gram per second is given by

$$\epsilon = \epsilon_{\text{nuc}} + \epsilon_g , \tag{B8}$$

where

$$\epsilon_g = \frac{P}{\rho^2} \frac{d\rho}{dt} - \frac{dU}{dt} .$$

Here, U is the internal energy per gram at any point in the star. The subscript g is slightly misleading since, strictly speaking, it is not ϵ_g but the quantity $(P/\rho^2)d\rho/dt$ which expresses the rate at which gravitational energy is made available locally. On integration over the entire star, $L_g = \int \epsilon_g \, dM$ represents the rate at which the total gravitational and thermal energy of the star decreases.

Given an equation of state relating ρ, P, and T, ϵ_g may be converted to the form

$$\epsilon_g = E_p \frac{dP}{dt} - C_p \frac{dT}{dt} , \tag{B9}$$

where E_p and C_p are functions of P and T. In evolutionary calculations, this expression is approximated, in the notation of Appendix A, by

$$(\epsilon_g)^{n+1}{}_{i-1/2} \cong (E_p)^{n+1}{}_{i-1/2} \frac{P^{n+1}{}_{i-1/2} - P^n{}_{i-1/2}}{\Delta t} - (C_p)^{n+1}{}_{i-1/2} \frac{T^{n+1}{}_{i-1/2} - T^n{}_{i-1/2}}{\Delta t} . \tag{B10}$$

In regions of the star where atoms are almost completely ionized, and electrons are not relativistically degenerate, the approximation of Henyey *et al.* (1959) to the equation of state is employed. With the definitions

$$\rho_0 = \frac{\mu M_{\text{H}}}{k} (P_g/T), \qquad \delta = 0.109754 (\rho/\mu_e T_6^{3/2}) ,$$

$$\lambda = \frac{\mu}{\mu_e} \delta / [5.01326(1 + 0.05512\,\delta)^{1/3}], \qquad \rho = \rho_0/(1 + \lambda) . \tag{B11}$$

Here, P_g = gas pressure, k = Boltzmann's gas constant, and μ = mean molecular weight. Defining

$$\psi = \lambda(\rho/\rho_0)(1 + \tfrac{2}{3} \times 0.05512\,\delta)/(1 + 0.05512\,\delta), \qquad \beta = P_g/P\,,$$
$$F = 4 - \beta(3 + 1.5\,\psi),\ G = 16 - \beta[12 + \beta\,(1.5 + 3.75\,\psi)]\,, \tag{B12}$$

one obtains the quantities needed in equation (19):

$$E_p = F/[\beta\rho(1 + \psi)], \qquad C_p = GP/[\beta\rho T(1 + \psi)]\,. \tag{B13}$$

The adiabatic temperature gradient $[d(\log T)/d(\log P)]_{\rm ad}$ is given by

$$V_{\rm ad} = F/G\,. \tag{B14}$$

In regions near the surface of the star where hydrogen and helium are partially ionized, degeneracy is neglected. The expressions given by Iben (1963*a*) have been generalized to include radiation pressure. Using the notation of this last reference, let

$$Z_1 = 1 + \mu X\left(\sum_i \xi_i U_{iP'}\right),$$
$$Z_2 = 1 + \mu X\left(\sum_i U_{iT'}\right), \tag{B15}$$
$$Z_3 = 1 + \mu X\left(\sum_i U_{iP'}\right).$$

When radiation pressure is important, the Z's are to be replaced by

$$Z_1' = Z_1 + \alpha Z_3\,, \qquad Z_2' = Z_2 + \alpha Z_3\,, \qquad Z_3' = Z_3\,, \tag{B16}$$

where

$$\alpha = 4(1 - \beta)/\beta\,.$$

The quantities $\bar{C}_p$, $V_{\rm ad}$, and V_ρ defined by Iben (1963*a*) are replaced by

$$\bar{C}_p' = \bar{C}_p + \alpha(3 + Z_2' + Z_1'), \qquad V_{\rm ad}' = Z_1'/(\beta\bar{C}_p'), \qquad V_\rho' = Z_3'/(\beta Z_2')\,. \tag{B17}$$

Finally, one has

$$C_p = \frac{k}{\mu M_{\rm H}}\bar{C}_p'\,, \qquad E_p = Z_1'/\rho\,. \tag{B18}$$

REFERENCES

Bahcall, J N 1962, *Phys Rev*, **128**, 1297.
Cameron, A. G W 1962, *Sky and Telescope*, **23**, 244.
Caughlan, G R and Fowler, W. A. 1964, *Ap. J.*, **139**, 1180.
Chandrasekhar, S. 1939, *An Introduction to the Study of Stellar Structure* (Chicago: University of Chicago Press), chap ix.
Eddington, A S 1926, *The Internal Constitution of the Stars* (Cambridge: Cambridge University Press), p 89.
Hayashi, C. 1961, *Pub. Astr Soc. Japan*, **13**, 450.
Hayashi, C , Hoshi, R., and Sugimoto, D. 1962, *Progr. Theoret. Phys* (Kyoto), **22**, 1.
Henyey, L. G , LeLevier, R , and Levée, R. D 1955, *Pub. A.S.P.*, **67**, 154.
———. 1959, *Ap. J.*, **129**, 2.
Henyey, L. G., Forbes, J. E , and Gould, N. L. 1964, *Ap. J.*, **139**, 306.
Iben, I , Jr 1963*a*, *Ap J.*, **138**, 452.
——— 1963*b*, Paper presented at NASA Conference on "Stellar Evolution" November 1963 (to be published in *The Proceedings of the Stellar Evolution Conference*, New York, 1963).

Iben, I , Jr., and Ehrman, J. R. 1962, *Ap. J.*, **135**, 770.
Kavanagh, R. W. 1958, *Bull. Amer. Phys. Soc.*, **3**, 316.
Kippenhahn, R., Temesvary, S., and Bierman, L. 1958, *Zs. f. Ap.*, **46**, 257.
Kuhi, L. V. 1964, *Ap. J.*, **140**, 1409.
Parker, P. D. 1963, unpublished Ph.D. thesis, California Institute of Technology.
Parker, P. D., Bahcall, J N., and Fowler, W. Z. 1964, *Ap. J.*, **139**, 602.
Salpeter, E. E. 1954, *Australian J. Phys.*, **7**, 373
Schwarzschild, M. 1958, *Structure and Evolution of the Stars* (Princeton, N.J.: Princeton University Press), chap. iv.
Weymann, R., and Moore, E. 1963, *Ap. J.*, **137**, 552.